

Analyzing Brain with Graphs

Bohan Wu*

Department of Statistics, Rice University

May 10, 2021

1 Introduction

Electrophysiological methods, such as electroencephalography (EEG) and magnetoencephalography (MEG), are used commonly in cognitive neuroscience. These approaches aim to understand the brain's network structure, which is traditionally thought to be believed distributed; e.g., an attention network has spatially remote nodes in the parietal and frontal cortex. Thanks to the recent advance in computing power, there has been a rising trend of using a data-driven approach to characterizing the brain network with measures of temporal correlation. Although much literature has explored brain networks, most of them focus on the more dominant, low-frequency component of brain signals, i.e., the "Alpha" signals. The literature on the high-frequency component, or "Gamma" signals, has been less reliable. Hence, the objective of our analysis is two-fold: first, we propose a reliable method to decompose the raw brain signals into "Alpha" and "Gamma" signals; second, we implement a temporal graphical model that provides insight into the temporal dependency amongst the brain regions.

In the neuroscience literature, the most common approach for estimating the network is through the concept of amplitude envelope correlation (Colclough et al. (2016)). However, the definition of amplitude envelope correlation is restrictive and can potentially lead to spurious network findings. An alternative approach is to treat the EEG data as high-dimensional multivariate time series and use high-dimensional time series models. It is useful to impose the additional assumption of sparsity.(e.g., Bühlmann and van de Geer (2011)). Another challenge specific to high-dimensional time series is to capture the complex within and between-series dependency. The solution is to use a high-dimensional vector autoregressive process. In particular, Basu and Michailidis (2015) established that consistent estimation

*The authors gratefully acknowledge

under high-dimensional scaling is possible via l_1 -regularization for vector autoregressive (VAR) models. Our objective is to confirm or question the believed connectivity network by applying the sparse time series model proposed by Basu and Michailidis (2015) to EEG brain data and compare our findings to the results obtained using amplitude envelope correlation to show that the sparse time series model is the superior model for the EEG data

2 Data Processing

The MEG data is recorded on over 200 experiment subjects between 55 and 88. The data is collected on 38 brain regions for each subject through a head-worn device with a 1000 Hz raw sampling rate. The distribution of the voxels is shown in Figure 1. The recording lasted for a duration of 9 minutes, throughout which the subject remains resting. After preprocessing, we obtain brain signal data with a 250 Hz sampling rate. Brain signals can be viewed as oscillating electrical voltages in the brain that measure just a few millionths of a volt. There are five main recognizable categories of brain signals, as explained in Table 1. From a neuroscience standpoint, it is common to decompose the brain wave signals into signals that belong to various frequency bands. Our analysis focuses on the temporal dependency of the "Gamma" brain signals, i.e., signals with frequency ≥ 35 Hz.

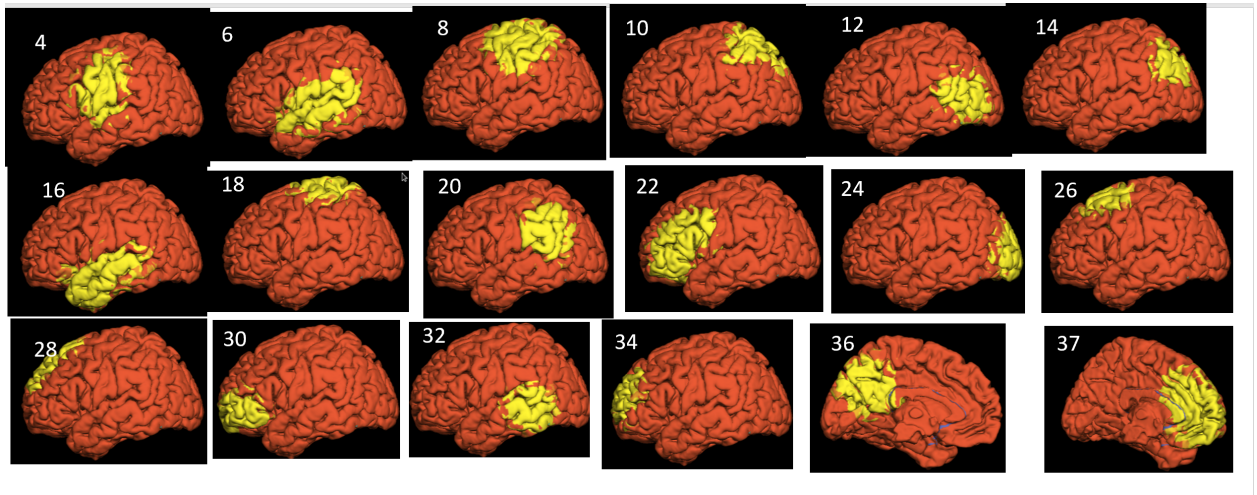


Figure 1: The locations of regions in the order of time-series in the data matrices. The skipped time series in the pics are from the right hemisphere in the same order.

Table 1: Five Categories of Brain Signals

Frequency Band	Frequency	Common Brain States
Gamma (γ)	≥ 35 HZ	Concentration
Beta (β)	12 – 35 HZ	Anxiety dominant, active, external attention, relaxed
Alpha (α)	8 – 12 HZ	Very relaxed, passive attention
Theta (θ)	4 – 8 HZ	Deeply relaxed, inward-focused
Delta (δ)	0.5 – 4 HZ	Sleep

Suppose we have a p -dimensional brain signal time series $[X^t] = \{(X_1^t, \dots, X_p^t)\}$ for a given subject. To extract the "Gamma" brain signal from the raw signals, we fit a smoothing spline model with smoothing parameter 0.5 to each time series X_j^t and subtract the smoothed fit \hat{X}_j^t to obtain the residual series X^{*t}_j , where $X^{*t}_j := X_j^t - \hat{X}_j^t$. The plot of spectral densities suggests that the smoothed fits captured the low-frequency components in the original signals, while the residuals series X^{*t} have only spectral densities at high frequency. Figure 2 show spectral densities of the p -dimensional smooth series $\hat{X}^t = \{\hat{X}_j^t\}_{j=1}^p$ and the p -dimensional residual series $\hat{X}^{*t} = \{X^{*t}_j\}_{j=1}^p$. The frequency of smooth series concentrates around 8 – 12 HZ, i.e., the "Alpha" range. After removing the smooth series, the frequency of the residual series shows no spectral density in the "Alpha" range. This shows that the smoothing splines approach succeeds in restricting $(X^*)^t$ to the "Gamma" and high "Beta" frequency bands, which we then use for implementing our analysis.

3 Methods

3.0.1 Amplitude Envelope Correlation

Neuroscientists use a variety of resting-state connectivity metrics to estimate the network. The most common approach is the amplitude envelope correlation (Colclough et al. (2016)). We estimated the amplitude coupling between ROIs using linear correlations and partial correlations of the envelopes of the band-pass filtered signals(Brookes et al., 2012; Hipp et al., 2012). Power envelopes were computed as the magnitude of the analytic signal, h , formed from the Hilbert transform of the ROI time-courses according to equation

$$h_j = X_j + i\hat{X}_j$$

where $\hat{X}_j = p.v. \int_{-\infty}^{\infty} d\tau \frac{s(\tau)}{t-\tau}$ is the Hilbert transform of signal X_j within each epoch and p. v. indicates the Cauchy principal value. The amplitude envelope correlation (AEC) is defined as the linear correlation is defined as the linear correlation between the logarithm of ROI power envelopes. For example, given two voxels with the (log) analytic signals h_x and h_y , the amplitude envelope correlation simply corresponds to the Pearson correlation coefficient r

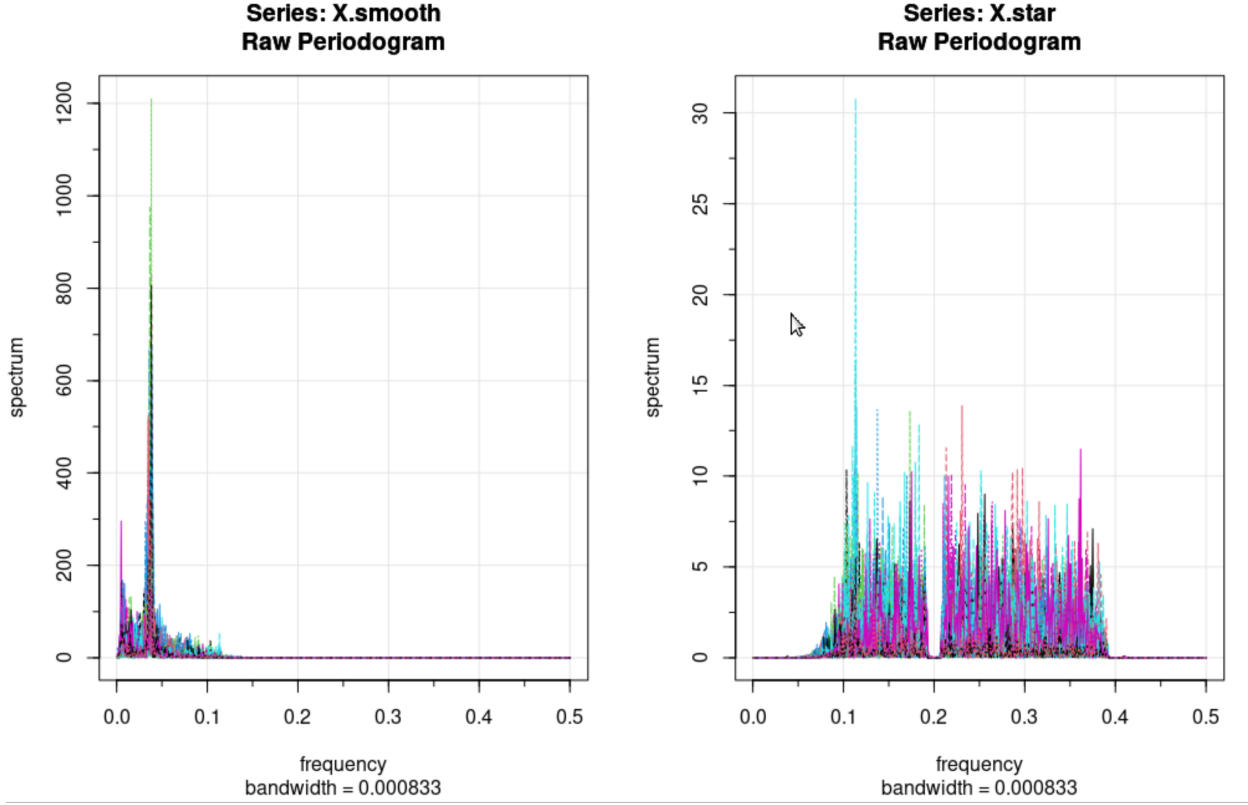


Figure 2: The periodograms of the p-dimensional smooth series and the p-dimensional residual series. $X.\text{smooth}$ denotes the smooth series and $X.\text{star}$ denotes the residual series. Each distinct color corresponds to a j^{th} component in the series. frequency (in HZ) = frequency (in periodogram) $\times 250$. For example, the frequency of 0.1 in the periodogram represents $0.1 \cdot 250 = 25\text{HZ}$.

of the two analytic signal series

$$r_{xy} = \frac{\text{cov}(h_x, h_y)}{\sqrt{\text{Var}(h_x)\text{Var}(h_y)}}$$

where $\text{Var}(h_x)\text{Var}(h_y)$ are the variance and $\text{cov}(h_x, h_y)$ is the covariance of the two analytic signal series.

After obtaining the amplitude envelope correlation matrix for the brain signals, we use the graphical Lasso (glasso) approach to estimate the high-dimensional undirected graph. Note that amplitude envelope correlation does not provide insights about the lead-lag relationship between time series, i.e., whether 1) x leads y , 2) y leads x , or 3) x, y are conditionally independent given a third variable. Analyzing these possibilities requires a model that

characterizes the causal relationship between time series at different lags. This motivates the use of vector autoregressive (VAR) models.

3.0.2 Sparse VAR

For a p -dimensional vector-valued stationary time series $[X^t] = \{(X_1^t, \dots, X_p^t)\}$, a VAR model of lag d [VAR(d)] with uncorrelated Gaussian errors take the form

$$X^t = A_1 X^{t-1} + \dots + A_d X^{t-d} + \epsilon^t, \epsilon^t \sim N(0, \Sigma_\epsilon)$$

where A_1, \dots, A_d are $p \times p$ matrices and ϵ^t is a p -dimensional vector of innovations. VAR estimate the transition matrix A_1, \dots, A_d based on the time series realization $[X^0, X^1, \dots, X^T]$. The structure of transition matrices gives us information about the temporal correlations amongst the p time series and provide also an efficient framework for forecasting.

The transition matrices A_1, \dots, A_d are estimated using l_1 -penalized least-square estimators to enforce the sparsity assumption. After obtaining the estimates of A_1, \dots, A_d , we put a threshold on the estimated transition matrices (in our example, we only look at $d = 1$) to create directed edges representing the past-present correlations between nodes. Similarly, we can put a threshold on the variance-covariance matrix Σ create undirected edges representing the present-present correlations between nodes. A parallel computing scheme is implemented for the model estimation.

4 Results

Due to time constraints, the analysis only looks at the brain signals from one subject. We will generalize the analysis to all subjects in the next stage of the project. Let $[X^t]$ be the 38-dimensional vector-valued brain signal time series of the subject. Furthermore, assume that $[X^t]$ is stationary.

After computing the amplitude envelope correlation matrix of $[X^t]$, we fit a sparse graphical model with Lasso (l_1) penalty on the AEC matrix to estimate the brain network structure. As seen in Figure 3, the AEC matrix with the glasso approach suffers from two problems 1) the graph gets sparse too quickly. The graph estimate goes from densely connected with a complex structure to extremely sparse with only the tree structure as lambda increases from 0.05 to 0.083. However, both dense structure and tree structure are unreliable from a neuroscience perspective. 2) the graph estimates fail to characterize the lead-lag relationship between brain regions. In comparison, the sparse VAR method can provide a decently sparse graph with both a large "clustering" structure and local tree structure. The large "clustering" structure represents the dominant functional network associated with the person's main brain state. For example, the memory network corresponds to "jogging up the memory"; the attention network corresponds to "paying attention." The small tree-like structure represents

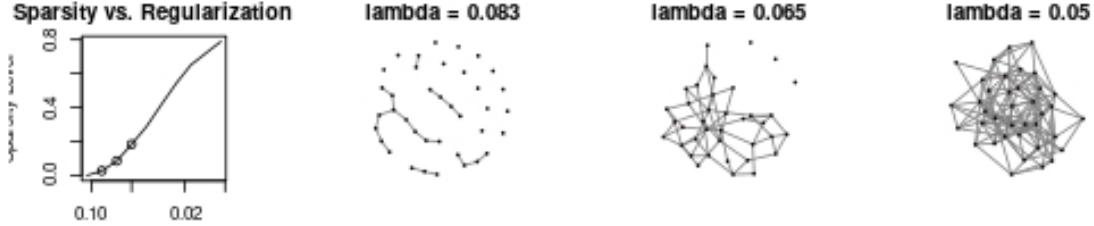


Figure 3: Undirected graph of the brain network estimated by applying graphical lasso (glasso) to the AEC matrix. Lambda is the tuning parameter fro the glasso estimation. Higher lambda value imposes more sparsity on the graph.

other brain activities that are either leftover from the preceding brain state or "random thoughts." Moreover, the sparse VAR method has the advantage of showing the lead-lag relationships between brain regions in the form of directed edges. For example, the directed edge from 9 to 33 means an information transfer from brain region 9 to region 33, but not otherwise. Hence, the sparse VAR method can inform us of the interesting dynamics of the "spreading" of brain activation within short time intervals. The information allows neuroscientists to quickly identify the brain regions that serve as "initiator," "receiver," and "hub" in a given network. See Figure 4.

5 Conclusion

We showed that the sparse VAR method proposed by Basu and Michialidis (2015) is the superior method for analyzing the high-frequency brain signals because 1) the network estimate of sparse VAR matches the neuroscience knowledge, and 2) sparse VAR characterizes information "spread" between brain regions, while graph estimated by conventional connectivity metrics cannot provide this information. Besides the model comparison, we proposed a data-driven smoothing spline approach to decompose the raw brain signals into "Alpha" and "Gamma" signals, which is quite useful for brain signal processing.

There are plenty of things that we did not get to in this project. For example, we would like to explore which regions participate in the different functional networks, how the network topology changes in a multi-lag setting, how the network structure morphs with old age, and verify whether Alzheimer disease patients have desynchronized network compared to healthy patients. For the next step, we will apply the sparse VAR method to different subjects and analyze the association between the directed brain network and age.

6 Reference

- Abhang, P., Gawali, B., Mehrotra, S. (2016). Technological Basics of EEG Recording and Operation of Apparatus. *Introduction To EEG- And Speech-Based Emotion Recognition*, 19-50.
- Basu, S., Michailidis, G. (2015). Regularized estimation in sparse high-dimensional time series models. *The Annals of Statistics*, 43(4), 1535-1567.
- Colclough GL, Woolrich MW, Tewarie PK, Brookes MJ, Quinn AJ, Smith SM. (2016). How reliable are MEG resting-state connectivity metrics? *Neuroimage*, 138:284-293.
- Sara van de Geer, Peter Bühlmann, Shuheng Zhou. (2011). The adaptive and the thresholded Lasso for potentially misspecified models (and a lower bound for the Lasso). *Electronic Journal of Statistics*, 5(none) 688-749.
- Sitnikova, T. A., Hughes, J. W., Ahlfors, S. P., Woolrich, M. W., Salat, D. H. (2018). Short timescale abnormalities in the states of spontaneous synchrony in the functional neural networks in Alzheimer's disease. *NeuroImage: Clinical*, 20, 128-152.

SUPPLEMENTAL MATERIALS

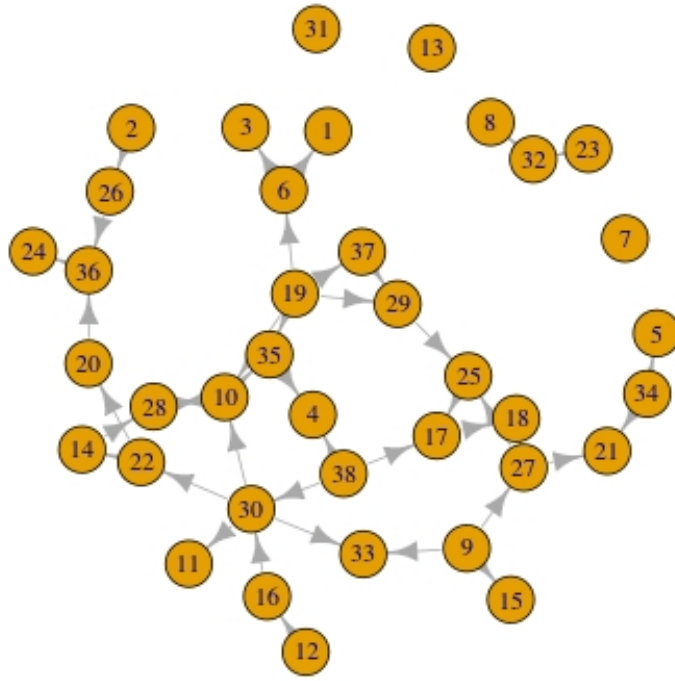


Figure 4: Directed graph of the brain network estimated with sparse VAR method (Basu and Michalidis, 2005) with threshold = 0.7. A directed edge (i, j) represents the information transfer from region i to region j .

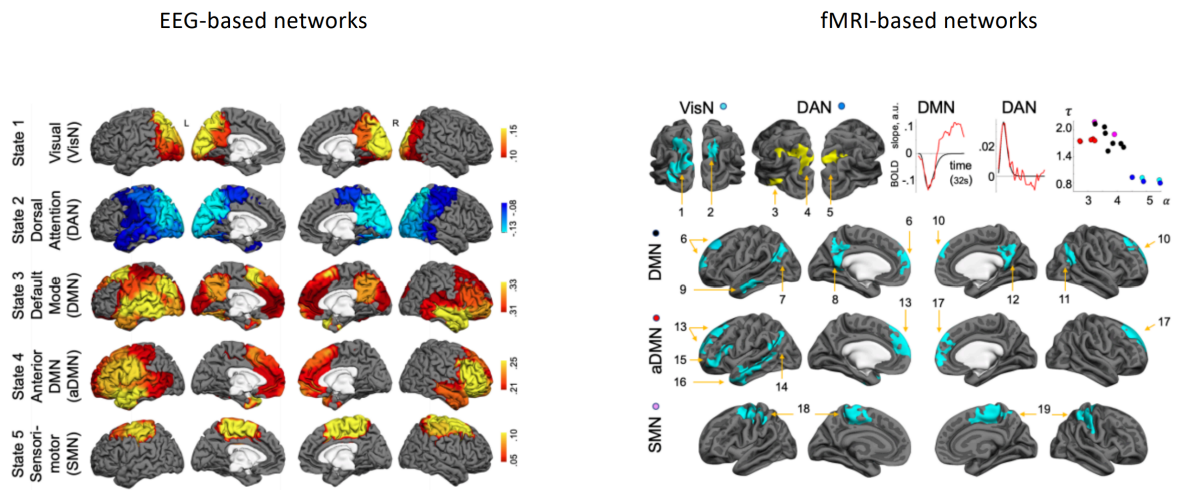


Figure 5: EEG-based networks vs. fMRI-based networks

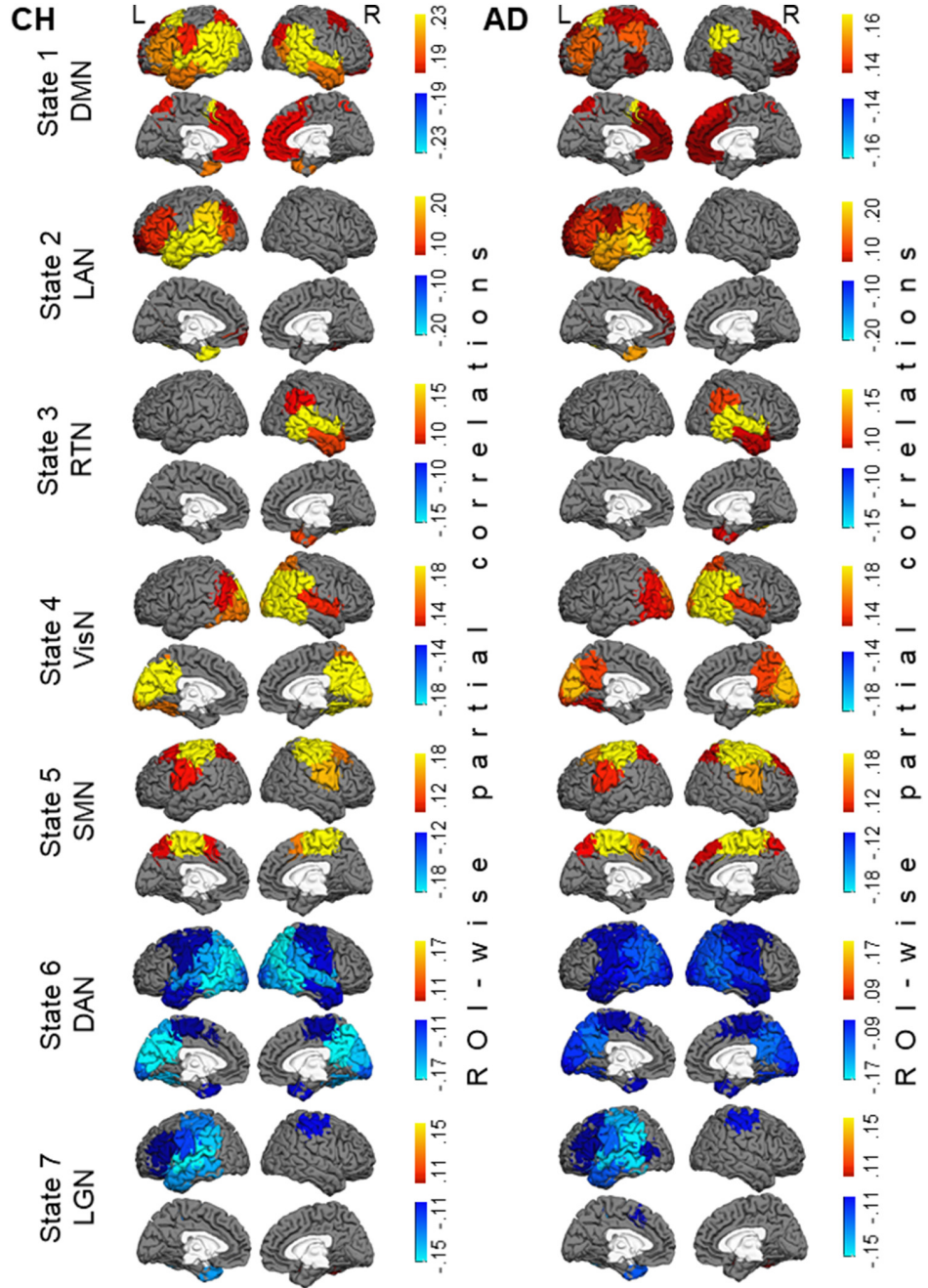


Figure 6: Maps of state-specific increases (in yellow/red/brown colors) and decreases (in blue color) in oscillatory amplitudes during seven network states. Maps in the CH group are shown in the left panel and in the AD group in the right panel. Abbreviations: CH, cognitively healthy, AD, Alzheimer's disease, DMN, default mode network, LAN, left associative network, RTN, right temporal network, VisN, visual network, SMN, sensorimotor network, DAN, dorsal attention network, LGN, language network